The Astrophysical Journal, 645:1264–1271, 2006 July 10
© 2006. The American Astronomical Society. All rights reserved. Printed in U.S.A.

OUTFLOWS FROM MASSIVE YOUNG STELLAR OBJECTS AS SEEN WITH THE INFRARED ARRAY CAMERA

Howard A. Smith, J. L. Hora, and M. Marengo
Harvard-Smithsonian Center for Astrophysics, 60 Garden Street, Cambridge, MA 02138; hsmith@cfa.harvard.edu

and

Judith L. Pipher
Department of Physics and Astronomy, University of Rochester, Rochester, NY 14627
Received 2006 January 18; accepted 2006 February 10

ABSTRACT

The bipolar outflow from the massive star-forming cluster in DR 21 is one of the most powerful known, and in IRAC images the outflow stands out by virtue of its brightness at 4.5 μm (band 2). Indeed, IRAC images of many Galactic and extragalactic star formation regions feature prominent band 2 morphologies. We have analyzed archival *ISO* SWS spectra of the DR 21 outflow and compare them to updated H_2 shocked and UV excitation models. We find that H_2 line emission contributes about 50% of the flux of the IRAC bands at 3.6, 4.5, and 5.8 μm, and is a significant contributor to the 8.0 μm band as well, and confirm that the outflow contains multiple excitation mechanisms. Other potentially strong features, in particular Brα and CO emission, have been suggested as contributing to IRAC fluxes in outflows, but they are weak or absent in DR 21; surprisingly, there also is no evidence for strong PAH emission. The results imply that IRAC images can be a powerful detector of, and diagnostic for, outflows caused by massive star formation activity in our Galaxy, and in other galaxies as well. They also suggest that IRAC color-color diagnostic diagrams may need to take into account the possible influence of these strong emission lines. IRAC images of the general ISM in the region, away from the outflow, are in approximate, but not precise, agreement with theoretical models.

Subject headings: infrared: ISM — ISM: individual (DR 21) — ISM: jets and outflows — ISM: molecules — stars: formation

Online material: color figures

1. INTRODUCTION

DR 21 contains one of the most massive star formation regions and molecular outflows in our galaxy. It is an excellent test bed for studying the conditions of massive star formation and for comparing competing ideas about the formation and subsequent evolution of massive new stars and their environments, for example, the relative roles of cloud collisions and fragmentation in these processes. The extended DR 21 nebula consists of a filamentary ridge of massive star-forming clusters that stretch from DR 21 (main) northward to W75N, and includes clusters around the bright maser source DR 21(OH). Along with the rest of the Cyg X complex in which it is embedded, DR 21 appears as part of a shell-like structure around the supermassive Cyg OB2 association. This association lies in the direction of a tangent to the Orion arm of the Galaxy, and as a result its distance is relatively difficult to estimate. T. M. Dame, using CO and H I maps of the galaxy, estimates the distance to Cyg OB2 as 1.7 kpc (2005, private communication; Butt et al. 2003). We adopt this value for DR 21 even though the most commonly used distance in the past literature has been 3 kpc. We thus revise downward a number of earlier estimates of luminosity, etc., so as to scale accurately to this closer distance.

The giant molecular outflow in DR 21 is one of the most powerful outflows in our Galaxy. An estimated driving force (estimated from the H_2 lines) of $\sim 5.5 \times 10^{30}$ dynes (Garden et al. 1986) exceeds the driving force of the Orion IRc2 outflow by almost a factor of 6 (Cabrit & Bertout 1986). The outflow velocity of about 60 km s^{-1} or more drives a mass estimated at >3000 $M_\odot$. The energy of the flow is in excess of 2×10^{48} ergs; the luminosity of the 2 μm H_2 flow alone has been calculated to be 1800 $L_\odot$, and, as we show below, the 2 μm lines are not even the brightest ones. Cyganowski et al. (2003) claim evidence for a second "highly collimated" flow perpendicular to the main one. In part because of the distance to DR 21, and also because of the high extinction there, our understanding of the complex has been somewhat limited. That DR 21 has regions of very high extinction was shown by Chandler et al. (1993a, 1993b), who use the CS line observations and 1.3 mm dust, respectively, to conclude that clumps exist with column densities as high as $N(\mathrm{H} + \mathrm{H_2}) \sim 3 \times 10^{24}$ cm^{-2}; $C^{18}O$ observations (Wilson & Mauersberger 1990) had provided estimates that were also substantial but about 10 times less. Adjusting to the closer distance of 1.7 kpc and converting to visual extinctions give an estimate in places of $A_V \sim 1000$. *Spitzer* Infrared Spectrograph (IRS) data on the embedded young protostar find a very deep CO_2 absorption also consistent with this estimate (H. A. Smith et al. 2006, in preparation). The *Infrared Astronomical Satellite* (*IRAS*) detected a very bright point source near the apparent source of the massive outflow, but identifying the actual source of the flow, a massive young stellar object (YSO), has proved elusive. Previous studies of the outflow region identified a source "IRS 1" as the driver for the outflow, but Infrared Array Camera (IRAC) images find no point source coincident with the *IRAS* location. Instead, we find one overwhelmingly strong 8.0 μm (band 4) point source located about 10″ from the position of the *K*-band star first dubbed IRS 1 (Davis & Smith 1996). This IRAC source was undetected at *K*; it is a young ~O7 star with $L_{\mathrm{FIR}} \sim 1.5 \times 10^5$ $L_\odot$, apparently still accreting from its envelope. A full description of the source and its environment is in H. A. Smith et al. (2006, in preparation). It is this source that is thought to power the immense bipolar outflow from the cloud.

The outflow has been imaged and studied in H_2 by numerous authors (e.g., Garden et al. 1986, 1990, 1991; Davis & Smith 1996; Fernandes et al. 1997). Fernandes et al. conclude that the 2 μm line ratios are best fit by a photodissociation region (PDR) model with a far-ultraviolet (FUV) field in the range of $2 < g < 3$ and a preshock density of $n = 3 \times 10^3$ cm^{-3}, and with a small shock contribution. Smith et al. (1998, hereafter S98) used the *Infrared Space Observatory*'s Short Wavelength Spectrometer (*ISO* SWS) to analyze five lines between 4.9 and 17 μm in one bright section of the outflow. They conclude there are both J- and C-type shocks at work in the region and distinguish this gas from the UV-excited gas at 2 μm modeled by Fernandes et al.

In this paper we present new IRAC images of the outflow region that dramatically reveal at 4.5 μm the structures seen by the 2 μm images with much higher spatial resolution. The original IRAC observations of this region (Marston et al. 2004) were partially saturated on the bright point sources, with some effect on the neighboring outflow region pixels; our new observations were taken in high dynamic range (HDR) and subarray mode. We also present and analyze archival *ISO* SWS spectra of the DR 21 outflow, material not published in the original S98 paper; we report the fluxes on an additional four H_2 lines, as well as the on the atomic hydrogen Brα recombination line, and limits to other line fluxes and features falling over nearly all of the wavelength coverage of the IRAC instrument. The results show that the *Spitzer* IRAC instrument is a superb probe of shocked structures because of the strength of the H_2 lines and the placement of the IRAC bandpasses.

2. OBSERVATIONS AND ANALYSIS

2.1. *IRAC Observations of the Outflow*

The original DR 21 IRAC observations were taken as an Early Release Observation (ERO) and published in Marston et al. (2004). We repeated those observations in HDR and subarray modes in regions around the bright point source and the outflow that had suffered from saturation effects. (See the *Spitzer* Observer's Manual ver. 6.0[1] for details of these observing modes, which read out the data in much shorter time intervals.) A full description of the point source and its nature will be presented elsewhere (H. A. Smith et al. 2006, in preparation). The data analyzed here were processed in pipeline S11.0.2. Figure 1 shows the IRAC 3.6/4.5/8.0 μm (bands 1, 2, and 4, respectively) color composite of the western lobe of the outflow region.

Davis & Smith (1996) obtained high-resolution, high signal-to-noise ratio (S/N) images of the H_2 1–0 $S(1)$ line emission from DR 21. It was this same Davis & Smith paper that most convincingly identified a bright 2 μm star as the source of the outflow. As we show in more detail (H. A. Smith et al. 2006, in preparation), this is an erroneous identification, and the actual driving star is located about 15″ away; it is not apparent in any K-band images but dominates the entire region at 8 μm. Davis & Smith used a narrowband ($\Delta\lambda = 0.02$ μm) filter centered at 2.12 μm to obtain their H_2 image, and also a wide-band K filter, and subtracted the scaled K-band image from the narrowband image to produce the line map. Their spatial resolution was 0.″63 pixel^{-1}. In Figure 2 we superimpose contours of their 1–0 $S(1)$ image on our (lower resolution) IRAC 4.5 μm (band 2) image. There is a nearly exact correspondence between the H_2 peaks and filaments and the 4.5 μm structures. This close correspondence across the $\sim$1 pc length of the flow suggests that the conclusions we draw from an analysis of the smaller *ISO* SWS field can be safely generalized to the entire shocked outflow. Superimposed on the image is the placement of the *ISO* SWS beam for the primary spectral observation, TDT 04402144—it is this region of the shock that we analyze in detail below.

2.2. *Infrared Space Observatory's Short Wavelength Spectrometer Observations*

ISO SWS obtained seven sets of observations of the DR 21 "west lobe" in addition to another 15 observations of varying quality centered elsewhere around the region. Wright et al. (1997) published an initial SWS analysis of the outflows in a short abstract and concluded that a combination of multiple shock components and some UV excitation were probably at work. S98 analyzed and published the results from one of the outflow observations, TDT 34700904, in their meticulous analysis of the H_2 emission from DR 21 West. That SWS observation, which was not a full-wavelength scan but rather a set of individual line scans, covered and obtained data on five of the H_2 lines: the 0–0 $S(1)$ at 17.03 μm, and four that fall in the IRAC coverage: the 0–0 $S(5)$ and 0–0 $S(7)$ lines, and the 1–1 $S(7)$ and 1–1 $S(9)$ lines. We reanalyzed that data set and are in agreement with all of their line fluxes except for the flux in the 0–0 $S(7)$ line, for which we measure a value 22% larger, more than the uncertainly in the data; we use our value below and note that the difference may be due to our use of a more recent pipeline processing and calibration. Based on the observed line strengths, and combined with 2 μm observations of H_2, S98 concluded that the excitation in the DR 21 outflow could not be produced by a simple C- or J-shock, and a range of shock strengths was needed. This conclusion was in contrast to the results of Fernandes et al. (1997), who relied on ground-based observations (only) to argue that the H_2 lines in the DR 21 outflow were best fit by a PDR model with an FUV field in the range of $2 < g < 3$ and preshocked density $n > 3 \times 10^3$ cm^{-3}. Smith & Rosen (2005) extended the Fernandes et al. analysis to simulate the *expected* images from IRAC observations under a wide range of shocked conditions.

We examined all seven sets of *ISO* SWS observations of the DR 21 west lobe outflow in an effort to try to understand the IRAC images more precisely. None of the SWS scans provided full, contiguous coverage. TDT 04402042 emphasized wavelengths over 10 μm, TDT 04402144 (Fig. 3 shows this spectral scan in the 7–9.5 μm interval) was contiguous from about 6.5 to 9.5 μm, and TDT 19301741 consisted of a series of some 21 short line scans between 2.2 and 36 μm. All these TDTs were taken at different epochs and included slightly different portions of the brightest part of the outflow, but all were centered roughly on the same part of the outflow, differing in location only by about 10″ (the latter TDT also used a larger beam size, 20″ × 33″). The new observation we use most, TDT 04402144, was centered 9.″4 to the northeast of the S98 slit and was rotated clockwise by 56°. None of these differences have any substantial effect on our rather general conclusions. The new TDTs we analyze here provide high-S/N fluxes on four *additional* H_2 lines in the IRAC wavelength coverage beyond the five analyzed in the S98 study: the 0–0 $S(9)$ and 0–0 $S(11)$ lines, the 1–1 $S(5)$ line, and the 1–0 $O(5)$ line. In addition, SWS detected the weak hydrogen recombination line Brα line at 4.052 μm and set useful limits on some others.

2.3. *The Strong* H_2 *Features*

The SWS spectral scan of the bright outflow over the 7–8.8 μm interval is presented in Figure 3. The H_2 0–0 $S(4)$ and $S(5)$ lines clearly dominate this interval. For all of the lines we calculate their corresponding fluxes in IRAC by converting each of the

[1] See http://ssc.spitzer.caltech.edu/documents/som/som60.pdf.

FIG. 1.—IRAC band 1 (3.6 μm, *blue*), band 2 (4.5 μm, *green*), and band 4 (8.0 μm, *red*) composite image of DR 21 (main). [*See the electronic edition of the Journal for a full color version of this figure*.]

observed line strengths into a flux density in the appropriate IRAC band using the IRAC instrumental response procedures as described in the IRAC Data Handbook (§ 5.2).[2] The Handbook, version 2.0, contains some significant errors in the Photometry and Calibration section (§ 5). In particular, the expression for converting flux into flux density (p. 41) is missing a wavelength ratio and should read $F = F_{\nu 0}(\mathrm{quot})\Delta\nu(\lambda/\lambda_0)/R_l$, and the Handbook, Table 5.2, lists inaccurate values for the bandwidth $\Delta\nu$ to be used in this expression; they are about 30%–40% too high in the version 2.0 table. We have used the corrected values (B. Reach 2006, private communication), as they appear in the new version of the Handbook (ver. 3.0). The flux density in the H_2 0–0 $S(4)$ line, converted to what it contributes to the IRAC 8.0 μm band, is 38.0 mJy. The 0–0 $S(5)$ line at 6.907 μm contributes another 66.0 mJy, making a total line flux density in the 8.0 μm band of 104 ± 10 mJy. All of the observed H_2 lines detected by *ISO* SWS observations are listed in Table 1.

[2] See http://ssc.spitzer.caltech.edu/irac/dh/iracdatahandbook3.0.pdf.

The results confirm that in the outflow region of DR 21 the H_2 lines contribute significantly to the IRAC band fluxes. We find that in the 4.5, 5.8, and 8.0 μm bands the *ISO* SWS *observed* line strengths alone account for between 13%–30% of the total measured IRAC fluxes (Table 2) in the outflow region studied by SWS (as indicated on Fig. 2); this value drops to about 6% for the 3.6 μm band. The slight uncertainties in the respective *ISO* measurements, for example, due to the slight rotations in the SWS beam between the different TDT observations of different lines, do not appreciably alter any of our conclusions. Figure 4 plots the measured IRAC flux densities summed over the region equivalent to the *ISO* SWS beam (*diamonds*), along with the contributions from the observed *ISO* SWS H_2 lines in those IRAC bands (*triangles*).

2.4. *The Faint Continuum and PAH Features*

Particularly worthy of notice in the mid-infrared (mid-IR) spectrum shown in Figure 3 (*top*) is the extremely faint continuum on which the H_2 lines sit, only about 0.93 ± 0.06 Jy. The complete

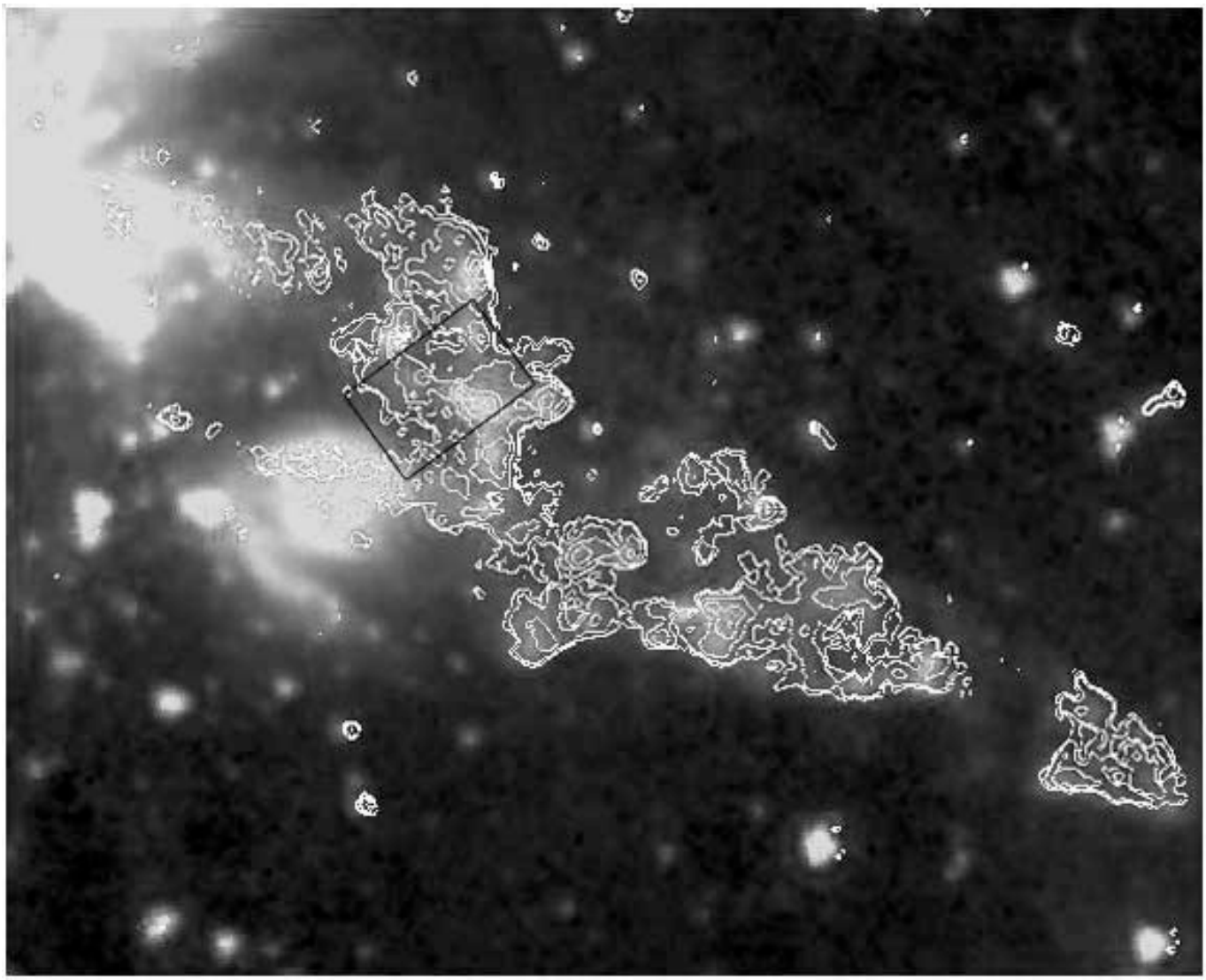

FIG. 2.—IRAC 4.5 μm band image, with the *K*-band H_2 1–2 *S*(1) line emission map overlaid in contours (from C. Davis 2005, private communication). There is a very close correspondence between the H_2 structures and the 4.5 μm band knots. The *ISO* SWS $14'' \times 20''$ field of view is outlined in black. [*See the electronic edition of the Journal for a color version of this figure*.]

absence of any characteristic sign of polycyclic aromatic hydrocarbon (PAH) emission features in the spectrum is striking. For comparison, Figure 3 (*bottom*) shows the spectrum of the bright region in DR 21 around the driving source about 40″ away. Here the strong PAH features completely dominate the spectrum, and the H_2 0–0 *S*(4) line, although present, is a peripheral feature. We were able to investigate the strength of the 3.4 μm PAH feature in the outflow as well, since two of the seven sets of SWS scans of the outflow did have marginally usable subscans over the this feature. In one scan (TDT 04402144) we were just able to detected the presence of this feature at 3 σ, at a level of $(1.2 \pm 0.4) \times 10^{-19}$ W cm^{-2}; it was undetectable in the others due to high noise. Figure 3 (*bottom*) of the main DR 21 cluster also shows clearly the emission lines from [Ar II] 6.985 μm, [Ar III] 8.991 μm, and the He II 12–10 line at 7.46 μm, that are excited by the embedded O star (H. A. Smith et al. 2006, in preparation).

The absence of PAH emission in the outflow was a surprise. It is well known that PAH features are weak or absent in the immediate vicinity of active galactic nuclei (AGNs) (e.g., Risaliti 2004; Lutz 2000), in some compact H II regions (Roelfsema et al. 1996), and in some planetary nebulae (Bernard-Salas & Tielens 2005). The reasons for these differences in PAH emission are not well understood. Strong ultraviolet radiation (energies over about 50 eV) will destroy PAHs (e.g., Risaliti 2004), for example, in the region of AGNs; dehydrogenated PAH species have weaker C-H bands (the 3.4 and 11.2 μm in particular; Pauzat et al. 1997; Verstrasete et al. 2001); and large PAHs ($N_{\rm carbon} > 100$) have dominant 6–16 μm features, while small ones dominate at 3.3 μm (Schutte et al. 1993). The ionization state is also a key parameter for PAHs. Hudgins & Allamandola (2004) provide extensive laboratory data that indicate the 5.8 and 8.0 μm band PAH features are comparatively very weak in neutral species but are strong in ionized PAHs. The example here of DR 21 West shows that PAH emission can change dramatically over only a few tenths of a parsec, as the environment changes from the neighborhood of a hot young massive star to the outflow of a rapidly moving shock. While it is clear that several types of processes are able to destroy or modify the PAH molecules in a way consistent with our observations, we cannot tell from our data alone which of these potential scenarios is the correct explanation. We will return to this general problem in the context of the general interstellar medium (ISM) in J. L. Hora et al. (2006, in preparation). For completeness, we note

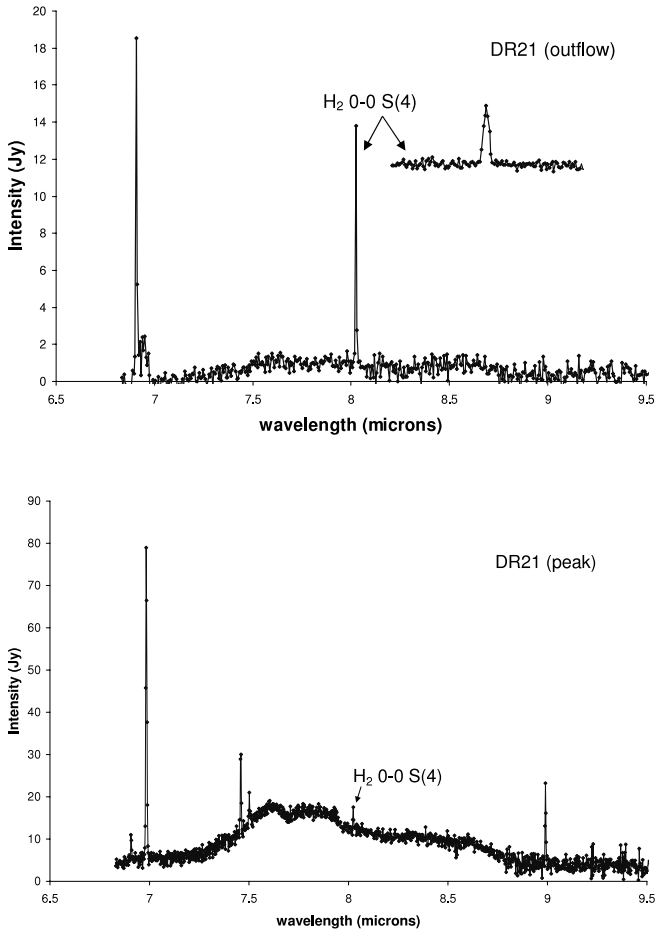

FIG. 3.—*Top:* Portion of the *ISO* SWS scan of the outflow. It shows the 0–0 *S*(4) emission line at 8.025 μm; the inset shows a zoom on this line. Note the very low continuum emission in the outflow. *Bottom:* In dramatic contrast to the outflow, the *ISO* SWS spectrum of DR 21 at the *peak* of the dust cloud shows strong continuum and PAH features, as well as lines of H_2, and atomic lines. The 0–0 *S*(4) line is visible but is not at all prominent.

that the zodiacal light contribution to the four bands at the epochs of observation is small; it is estimated by *Spitzer* as being 0.2, 1.0, 9.3, and 26.9 mJy, respectively, for bands 1–4.

2.5. *The Unseen Features: Brα and* CO

IRAC images of star formation regions and other nebulosity-rich objects often reveal strong 4.5 μm band emission, which is easily spotted as bright green nebulosity in three-color IRAC images in which the 4.5 μm band is coded (typically) as green.

TABLE 1
FLUXES OF THE *ISO* SWS–OBSERVED H_2 LINES

Line ID	Wavelength (μm)	Observed flux (10^{-15} W m^{-2})	Flux Contribution to IRAC Bands (mJy)
0–0 *S*(4).....	8.0250	4.80 ± 0.16	38.0
0–0 *S*(5).....	6.9091	11.5 ± 1.6	66.0
1–1 *S*(7).....	5.8111	0.13 ± 0.02	1.1
0–0 *S*(7).....	5.5115	6.50 ± 0.19	45.5
1–1 *S*(9).....	4.9533	0.15 ± 0.02	0.91
0–0 *S*(9).....	4.6947	1.81 ± 0.08	13.0
0–0 *S*(11).....	4.181	1.18 ± 0.2	7.2
1–0 *O*(5).....	3.235	0.54 ± 0.04	2.6

TABLE 2
IRAC FLUXES

IRAC Band	Wavelength (μm)	IRAC Fluxes[1] (mJy)	Observed H_2 Lines[b] (mJy)	Modeled H_2 Lines[c] (mJy)
1.....	3.6	46	2.6	25
2.....	4.5	71	21.1	34
3.....	5.8	320	46.6	123
4.....	8.0	760	104.0	151

[a] IRAC fluxes in a beam corresponding to the *ISO* SWS beam (14″ × 20″).
[b] H_2 lines observed by *ISO* SWS and converted to flux densities in the IRAC beam as described in the text.
[c] The sum of all of the H_2 lines in the IRAC bands from two models, one shock and one UV excited, as described in the text.

Churchwell et al. (2004), in their analysis of reflection nebula RCW 49, see just such bright 4.5 μm band emission. They conclude that the atomic hydrogen Brα line at 4.052 μm provides about 20% of the nonstellar flux in the 4.5 μm band, dominating the extended emission in that source. In the case of DR 21, however, we measure the Brα line with SWS to be $(1.6 \pm 0.4) \times 10^{-16}$ W m^{-2}, making it among the weakest of the emission lines in the outflow within the 4.5 μm band window, and 10 times weaker than the H_2 0–0 *S*(9) line. No other hydrogen recombination lines are seen in the SWS spectra of the outflow lobe. We conclude that "green nebulosity," insofar as it resembles shocked outflows like DR 21, signifies the presence of H_2, not Brα.

Geballe & Garden (1987, 1990) used the United Kingdom Infrared Telescope to obtain spectra of the Orion shocked outflow at 4.74 μm, the wavelength of the CO 1–0 *P*(8) line. They find it has a strength about $\frac{1}{10}$ of the strength of the H_2 0–0 *S*(9) line there and conclude, in agreement with some earlier observers, that shocked CO is an important contributor to the emission in the Orion outflow. Van Dishoeck et al. (1998) and Rosenthal et al. (2000) published an *ISO* SWS scan of the Orion IRc2 region, which includes the region studied by Geballe & Garden; they reported seeing CO emissioned in the 4.4–4.8 μm region. In the *ISO* SWS scans of the DR 21 West outflow, however, no CO lines are

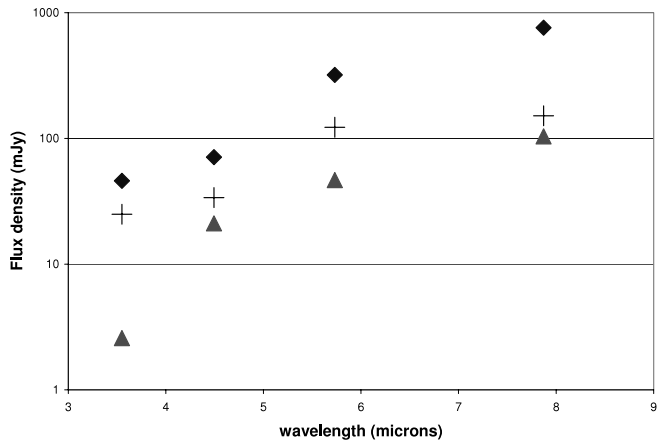

FIG. 4.—Comparison of the measured and modeled flux densities. The observed IRAC flux densities in the DR 21 outflow, measured in the same beam as the *ISO* SWS spectral observations, are plotted as diamonds; the observed SWS line fluxes per band, converted to IRAC flux densities, are plotted as triangles. The plus signs show the fit of a combined shock plus UV excitation model; each of these was normalized to one strong, observed line as described in the text; the residual flux is from the continuum. The 3 σ statistical uncertainties for all of the observations are approximately the same sizes as the data markers. [*See the electronic edition of the Journal for a color version of this figure.*]

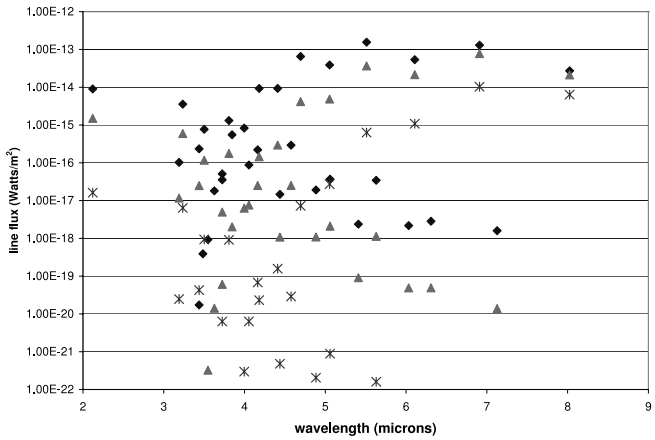

FIG. 5.—For the case of a preshocked density of 10^4 cm^{-3}, brightest shocked lines in the IRAC bandpasses vs. wavelength for shock velocities of 40 km s^{-1} (*diamonds*), 30 km s^{-1} (*triangles*), and 20 km s^{-1} (*asterisks*) (M. J. Kaufman 2005, private communication). [*See the electronic edition of the Journal for a color version of this figure.*]

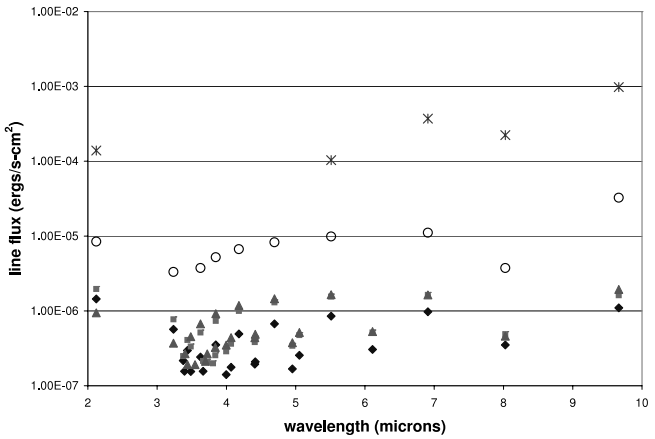

FIG. 6.—Brightest 90% of the H_2 lines in the PDR excitation models (M. G. Wolfire 2005, private communication) The five models shown are $n = 5$, $g = 4$ (*asterisks*), $n = 4$, $g = 4$ (*circles*), $n = 3$, $g = 5$ (*triangles*), $n = 3$, $g = 3$ (*squares*), and $n = 3$, $g = 2$ (*diamonds*). [*See the electronic edition of the Journal for a color version of this figure.*]

detected to a limit of about 3×10^{-16} W m^{-2}—less than about 16% of the nearby H_2 0–0 $S(9)$ line.

3. MODELS of the H_2 EMISSION

3.1. *Shock and PDR Models of the Outflow*

There are about 140 emission lines of H_2 in the IRAC bands whose strengths, depending on the model details, are within 1% of the strength of the strongest line in each excitation case. M. Kaufman and M. Wolfire have provided us with their as yet unpublished results of updated PDR and shock models (Kaufman et al. 2005; see also Kaufman & Neufeld 1996 and Wolfire et al. 1990). Figure 5 plots the brightest H_2 lines in the IRAC bands for the case of a preshocked density of 1×10^4 cm^{-3} moving with one of three different velocities, 20 km s^{-1} (*asterisks*), 30 km s^{-1} (*triangles*), and 40 km s^{-1} (*diamonds*). As might be expected, the strongest velocities produce by far the strongest line emission. It is also notable that the strongest velocities have the *least* flux variation in line fluxes across the IRAC bands, whereas the weaker velocities produce emission lines whose contributions between the IRAC bands vary much more substantively.

Fernandes et al. (1997), in their earlier analyses of ground-based observations of the DR 21 outflow, concluded that the DR 21 H_2 line ratios were best fit by PDR models because of the strength of the lines originating from the upper state $v = 2, 3$, and 4 levels; these are preferentially populated via nonthermal mechanisms, although there they also found a low-excitation shocked component. Figure 6 plots the brightest 90% of the bright H_2 lines predicted by M. Wolfire and M. Kaufman in the IRAC bands for five different cases of density n and ultraviolet flux g (where g is the log of the flux in units of the local interstellar FUV radiation, taken as 2×10^{11} photons s^{-2} m^{-2}). The strongest emission obviously comes from the most dense, highest UV regions, with the 8.0 μm band encompassing the brightest lines and the 3.6 μm band the faintest ones. However, it is noteworthy that there are many more detectable lines in the shorter bands, whose cumulative contributions can be substantial.

The four new H_2 lines in DR 21 we present here, the 0–0 $S(9)$, 0–0 $S(11)$, 1–1 $S(5)$, and 1–0 $O(5)$ lines, and the limits we can set to some lines *not* seen, allow us to make additional statements about the excitation mechanisms. Fernandes et al. (1997) concluded from their data that the most likely dominant excitation in DR 21 is from an FUV field with $2 \leq g \leq 3$ and a preshock density of $n \geq 3 \times 10^3$ cm^{-3}. The PDR model most analogous to the model parameters we have ($n = 3$, $g = 3$) predicts in that case a strength for the 4–3 $O(3)$ line at 3.3765 μm (one of the strongest discriminating H_2 lines) of 1.0×10^{-18} W m^{-2}. We set a limit from our analysis of the *ISO* SWS spectrum that is about 50 times fainter, thereby ruling out this case. Higher densities or UV flux values will reduce the predicted line flux ratio, and in the case of $n = 5$, $g = 4$ the 4–3 $O(3)$ line is about 150 times weaker, consistent with the new observational limit. However, in this case the longer wavelength lines, including the $v = 0$ pure rotational series, become very bright. We conclude that the most likely average PDR situation is more consistent with an $n = 4$, $g = 4$, and we take this as our baseline UV case for modeling. The new lines also add some additional consistency to the shock models. S98 concluded a mixture of C and J shocks were present. For our purposes, a shock with density of 10^4 cm^{-3} and a velocity of 30 km s^{-1} gives reasonable fits. In the more rapid shocks the relative contribution of H_2 lines to the 4.5 μm band lines is increasingly dominant, in part because this band (and the 3.6 μm band) includes a considerably larger number of weaker lines that are excited more effectively only at higher velocities, as was seen in the UV-excited scenario. But the higher velocity shocks are also intrinsically brighter.

The contribution of the *observed* H_2 lines to the IRAC band flux densities are listed in Table 1. We wanted to estimate the total contribution of the H_2 emission to the IRAC bands, because the *ISO* SWS scans were relatively sparse, in bands 1 and 2 especially. Our IRAC image (Fig. 1), as well as the 2 μm image (Fig. 2), show that the shocked H_2 emission in the outflow encompassed by the beam of *ISO* SWS includes many small knots. The calculated H_2 line brightness tables by M. Kaufman must therefore be corrected by appropriate, and somewhat uncertain, dilution factors when comparing absolute model flux predictions to the SWS observations presented in the tables. To make our estimate, we therefore normalized a shock model with density of 10^4 cm^{-3} and a velocity of 30 km s^{-1} to the strong, observed 0–0 $S(4)$ line, and we scaled a $n = 4$, $g = 4$ UV-excitation component to the strong, observed 1–1 $S(7)$ line—a line that is very weak in all shocked models. We then calculated the contribution of all of the H_2 lines to the IRAC bands from this combined model. The results are plotted in Figure 4 as plus signs. As expected, the modeled lines add considerable flux density, especially in the 3.6 μm band. When taking into account the H_2 lines that were not observed

directly by *ISO* SWS, the H_2 lines contribute about 50% of the total flux in IRAC 3.6, 4.5, and 5.8 μm bands; in the 8.0 μm band the lines contribute about 20% of the flux.

Some of the individual, observed line fluxes do not match the intensities predicted by this simple, two-component, normalized model, especially in the short-wavelength band. Adding other C-shock components from higher density regions could provide a solution, since at higher densities (as noted earlier) it is precisely the 3.6 and 4.5 μm fluxes that are most increased. S98 concluded that it was not possible to use a single shock model to explain the *ISO* SWS and ground-based lines they measured. Instead, they propose that a combination of C-type bow shocks with "wide flanks," together with localized extinction, can provide a consistent picture of the region. Alternatively, some component of low-density PDR emission might accomplish the same thing, but would require a larger filling factor and a more careful analysis to explain the absence of the 4–3 *O*(3) line. Our own data do not allow us to say much more the details of modeling, but neither will adjustments alter our main conclusion: that the H_2 lines play a major role in determining the IRAC fluxes and consequently the colors of the IRAC images.

3.2. *The Character of the ISM in DR 21 as Determined by IRAC*

Up to now we have analyzed the outflow in the region of the observed *ISO* SWS beam treated as an averaged whole. There is every reason to suspect, however, that additional details of the shock's structure can be revealed in the relative IRAC colors of the various knots and filaments. Figure 7 shows an IRAC color-color plot with all of the pixels in the giant outflow (*gray points*) and in the surrounding, unshocked nebulosity (*black circles*), given in magnitudes in order to be most useful for comparison with point-source colors. The uncertainties in the colors of the fainter, diffuse nebulosity are larger than those in the bright knots, but do not affect our conclusions.

The colors of the emission of the outflow itself form a narrow locus of points stretching from a [3.6]−[4.5] color of 1.5 mag in the top left of the color-color plot, down to a [5.8]−[8.0] color of 1.8 in the lower center. This locus is roughly the same as that produced by shocked H_2 lines alone, with preshock density of 1×10^4 cm^{-3}, when the range of velocities varies from 20 to 40 km s^{-1}; the top left portion corresponds to those lines originating from the fastest material. When the outflow is subdivided in smaller regions and their colors are separately considered, it is apparent that this range of colors is roughly the same in each zone. It is already clear from the work of S98 that multiple shock components are present; the variable colors across the flow simply confirm that complex and changing conditions are present.

There is one region in the outflow that is different from the others: the faintest part of the outflow—viz., the region at the western tip—is lacking in the reddest [3.6]−[4.5] gas, and instead has gas whose color lies only between about 0.6 and 1.2 mag. We do not have spectra of the western tip, but we note that decreasing the preshock velocity by about 10 km s^{-1} will decrease the cumulative line flux ratio in these bands in the most probable, low-density case, by a factor of ~5. It does so largely by reducing the 4.5 μm band line emission. Although the line contributions to this band and the 3.6 μm band are only about 50% of the total flux in the bands, the changes will bring the color closer to that observed. Increasing the densities by a factor of 10 can accomplish about the same thing in the higher velocity cases.

The background nebulosity, away from the massive strong outflow, is also of considerable interest, and we have also examined its IRAC colors. Figure 7 plots the colors of the nonoutflow

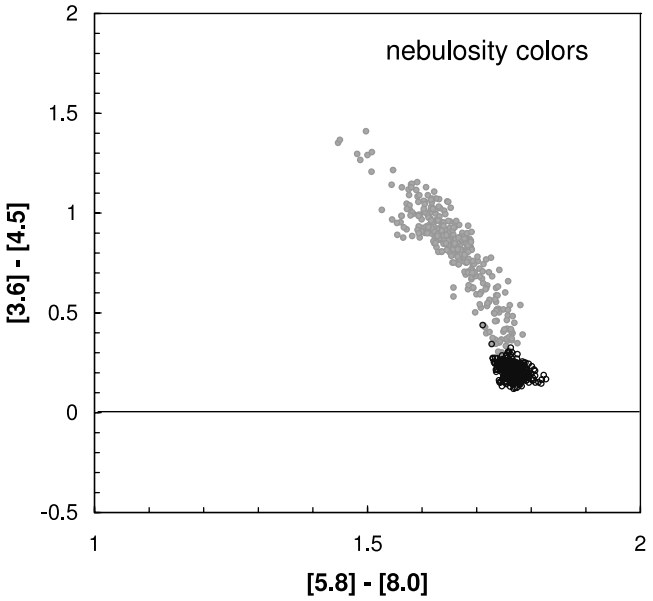

FIG. 7.—IRAC colors of the shocked outflow nebulosity (*gray points*) and surrounding nebulosity (*black circles*). The points correspond to 2×2 averaged IRAC pixels across the outflow. Analysis by subregion finds that all parts of the flow except one have roughly the same range of pixel colors; the westernmost tip is lacking the red [3.6]−[4.5] points with values above 0.6. The crosses correspond to pixels away from the outflow, in the general DR 21 nebulosity. The expected IRAC colors of diffuse nebulosity from the Li & Draine (2001) ISM models fall in the plot around the value (2.1, −0.35), appreciably removed from the observed locus in DR 21. [*See the electronic edition of the Journal for a color version of this figure.*]

nebulosity. The IRAC images away from the outflow are obviously less "green" in appearance when weighed with the customary three-band combinations, meaning less intense H_2 emission in the 4.6 μm band. Since the total flux densities are also much smaller away from the flow, we have averaged these nebular regions over much larger areas than were used in the outflow itself. All of the nonoutflow, nebulous regions are characterized by very modest reddening in the 3.6 and 4.5 μm bands—typically a color less than $[3.6] - [4.5] < 0.4$ mag; this is in contrast to values of 1.0 or greater in the outflow region. Red [3.6]−[4.5] colors are as strong an indicator of shock activity as strong 4.5 μm emission. In contract, the [5.8]−[8.0] colors of the diffuse nebulosity are virtually indistinguishable from the average colors in the outflow itself. Within the diffuse material there is a slight tendency for faint material to be even redder than brighter nebulosity, perhaps suggesting that UV, which excites the PAH emission there, plays a more dominant role in these regions. Draine & Li (2001) provide detailed quantitative models for the ISM in which they include PAH, silicate grain, and carbonaceous grain emission. Their Table 5 provides estimated, normalized flux densities for a range of seven values of the UV radiation field strength, $\chi_{\rm MMP}$, between 0.3 and 10^4. The IRAC colors of all these seven scenarios are about the same: $[3.6] - [4.5] \approx 0.35$, $[5.8] - [8.0] \approx 2.1$. The points are considerably bluer in [3.6]−[4.5], by a factor of at least 60%, than all but the bluest of nebular regions in our image; the band [5.8]−[8.0] color is about 0.25 mag redder than we observe. A more complete discussion of the IRAC properties of the ISM, including a more detailed analysis of the ISM in the DR 21 region, will be presented in J. L. Hora et al. (2006, in preparation).

4. CONCLUSIONS

Spitzer IRAC color images of star formation regions, typically coded with the 4.5 μm band as green, often show dramatic

swaths of green nebulosity. In the case of the massive outflow in DR 21, that "green monster" is seen largely thanks to the strong lines of shocked or UV-pumped H_2. Because the 4.5 μm band lacks strong PAH features such as can dominate the 5.8 and 8.0 μm bands, when composite IRAC images are scaled down (and corrected for bright point sources) so that the bright PAH regions do not overwhelm the image, the outflows show up as green nebulosity.

The *ISO* SWS spectra of the DR 21 western outflow lobe have allowed us to determine not only that H_2 is the overwhelming contributor to the outflow emission lines, they also enable us (in agreement with earlier analyses) to conclude that some combination of modest velocity C-shocks in a medium whose preshock density is between 10^3 and 10^4 cm^{-3}, coupled with some UV excitation in a region of similar density and a UV field characterized by $g = 4$, are the mechanisms responsible. We have not only found that the H_2 emission in the outflow is strong—we have found that the continuum emission is very weak. The implications, to be discussed further in the larger context of the DR 21 star formation complex and sources (H. A. Smith et al. 2006, in preparation), is that neither dust nor hot PAH molecules are abundant in this outflow. The *ISO* SWS spectra of the outflow contain no strong PAH features, no CO band head emission, and only very weak Brα emission.

IRAC color-color diagrams of the emission from regions across the outflow confirm the conclusions from the individual band flux analyses. In particular, the short-wavelength colors in the flow are consistently redder than are the colors of the nonoutflow, nonshocked ISM. Combined with shock models, the colors indicate that the shock at the western tip is likely to involve slower, denser material. The colors of the background nebulosity, away from the massive strong outflow, are characterized by very modest reddening between the 3.6 and 4.5 μm bands. They are mild disagreement with theoretical predictions of for ISM colors in both [3.6]−[4.5] and [5.8]−[8.0] colors.

IRAC images have made it relatively easy for scientists to spot small regions of the 4.5 μm band activity in otherwise large and complex fields. While the *Spitzer* IRS spectrometer cannot see the H_2 lines below 5 μm, its sensitive performance ought to enable a self-consistent picture to emerge from the other, longer wavelength H_2 lines that do fall in its windows. Both the strength of the 4.5 μm band and the [3.6]−[4.5] color are useful diagnostics of H_2 emission. The overall results indicate that IRAC images can be a powerful indicator of outflows caused by star formation activity. The results also suggest that IRAC color-color diagnostic diagrams for the nebulosity in star formation regions may sometimes need to take into account the possible influence of these strong H_2 emission lines, especially in cases when a large, extended emission is seen around an optically thick point source. It remains to be determined to what the extent the $\sim$140 H_2 emission lines across the IRAC bands contribute to the IRAC images of other star formation regions (or for that matter of other bright nebulae, like planetary nebulae, objects that are already known to be strong H_2 emitters).

We gratefully thank Mark Wolfire and Michael Kaufman for providing us with their latest calculations of the H_2 line strengths. We also thank Chris Davis for providing unpublished data on his 2 μm H_2 images. H. A. S. acknowledges partial support from NASA grant NAG5-10654. This work is based in part on observations made with the *Spitzer Space Telescope*, which is operated by the Jet Propulsion Laboratory (JPL), California Institute of Technology under NASA contract 1407. Support for the IRAC instrument was provided by NASA through contract 960541 issued by JPL. This work is also based in part on observations made with *ISO*, an ESA project with the participation of NASA and ISAS.

REFERENCES

Bernard-Salas, J., & Tielens, A. G. G. M. 2005, A&A, 431, 523
Butt, Y. M., et al. 2003, ApJ, 597, 494
Cabrit, S., & Bertout, C. 1986, ApJ, 307, 313
Chandler, C. J., Carlstrom, J. E., Scoville, N. Z., Dent, W. R. F., & Geballe, T. R. 1993a, ApJ, 412, L71
Chandler, C. J., Gear, W. K., & Chini, R. 1993b, MNRAS, 260, 337
Churchwell, E., et al. 2004, ApJS, 154, 322
Cyganowski, C. J., Reid, M. J., Fish, V. L., & Ho, P. T. P. 2003, ApJ, 596, 344
Davis, C. J., & Smith, M. D. 1996, A&A, 310, 961
Draine, B., & Li, A. 2001, ApJ, 551, 807
Fernandes, A. J. L., Brand, P. W. J. L., & Burton, M. G. 1997, MNRAS, 290, 216
Garden, R. P., Geballe, T. R., Gatley, I., & Nadeau, D. 1986, MNRAS, 220, 203
———. 1991, ApJ, 366, 474
Garden, R. P., Russell, A. P. G., & Burton, M. G. 1990, ApJ, 354, 232
Geballe, T. R., & Garden, R. P. 1987, ApJ, 317, L107
———. 1990, ApJ, 365, 602
Hudgins, D. M. & Allamandola, L. J. 2004, in ASP Conf. Ser. 309, Astrophysics of Dust, ed A. N. Witt, G. C. Clayton, & B. T. Draine (San Francisco: ASP), 665
Kaufman, M. J., & Neufeld, D. A. 1996, ApJ, 456, 611
Kaufman, M. J., Wolfire, M. G., & Hollenbach, D. J. 2005, preprint
Li, A., & Draine, B. T. 2001, ApJ, 554, 778
Lutz, D. 2000, NewA Rev., 44, 241
Marston, A. P., et al. 2004, ApJS, 154, 333
Pauzat, F., Talbi, D., & Bellinger, Y. 1997, A&A, 319, 318
Risaliti, G. 2004, in IAU Symp. 222, The Interplay among Black Holes, Stars and ISM in Galactic Nuclei, ed. T. Storchi-Bergmann, L. C. Ho, & H. R. Schmitt (Cambridge: Cambridge Univ. Press), 361
Roelfsema, P. R., et al. 1996, A&A, 315, L289
Rosenthal, D., Bertoldi, F., & Drapatz, S. 2000, A&A, 356, 705
Schutte, W. A., Tielens, A. G. G. M., & Allamandola, L. J. 1993, ApJ, 415, 397
Smith, M. D., Eisloffel, J., & Davis, C. J. 1998, MNRAS, 297, 687 (S98)
Smith, M. D., & Rosen, A. 2005, MNRAS, 357, 1370
van Dishoeck, E. F., Wright, C. M., Cernicharo, J., Gonzalez-Alfonso, E., de Graauw, T., Helmich, F. P., & Vendenbussche, B. 1998, ApJ, 502, L173
Verstraete, L., et al. 2001, A&A, 372, 981
Wilson, T. L., & Mauersberger, R. 1990, A&A, 239, 305
Wolfire, M. G., Tielens, A. G. G. M., & Hollenbach, D. 1990, ApJ, 358, 116
Wright, C. M., Timmerman, R., & Drapatz, S. 1997, in Proc. First *ISO* Workshop on Analytical Spectroscopy, ed. A. M. Heras et al. (Noordwijk: ESA), 311